geotechnics

MDPI

Article

Influence of Saline Pore Fluid on Soil Behavior during Evaporation

Jared Suchan and Shahid Azam *

Environmental Systems Engineering Faculty of Engineering and Applied Science, University of Regina, 3737 Wascana Parkway, Regina, SK S4S 0A2, Canada
* Correspondence: shahid.azam@uregina.ca

Abstract: Saline conditions govern soil behavior during evaporation, thereby affecting the water budget in semi-arid regions. This research examined the effects of saline pore fluid on soil behavior during evaporation. The results indicated volumetric reductions of about 5% for silty sand and about 15% for lean clay. The evaporative flux for silty sand decreased from 26 mg/m^2·s to 22 mg/m^2·s in *Stage II*, remained at a constant flux in *Stage III*, and decreased to 13 mg/m^2·s in *Stage IV*. The air entry and residual suction values were found to be 5 kPa and 100 kPa, respectively, and the total suction of about 5000 kPa merged with matric suction near the *Stage II*/*Stage III* boundary. The swell–shrink curve (SSC) was J-shaped with the only void ratio decrease in *Stage II*. In contrast, the evaporative flux for lean clay decreased from 30 mg/m^2·s to 15 mg/m^2·s in *Stage II*, to 10 mg/m^2·s in *Stage III*, and then to 5 mg/m^2·s in *Stage IV*. The air entry and residual suction values were 5 kPa and 2000 kPa, respectively, and the total suction during *Stage II* and *Stage III* ranged from 1000 kPa to 6000 kPa, with an average value of 3500 kPa. The SSC showed a major void ratio decrease in *Stage II*, marginal decrease in *Stage III*, and no decrease in *Stage IV*. Under high demand, the evaporative flux for silty sand was constant at 180 mg/m^2·s in *Stage III* and decreased to 50 mg/m^2·s in *Stage IV*, whereas it decreased for the lean clay from 230 mg/m^2·s to 145 mg/m^2·s in *Stage II*, to 95 mg/m^2·s in *Stage III*, and then to 25 mg/m^2·s in *Stage IV*. For both soils, the total water loss was found to be six times higher than that under low demand.

Keywords: evaporative flux; water retention; saline pore fluid; soil shrinkage

check for updates

Citation: Suchan, J.; Azam, S. Influence of Saline Pore Fluid on Soil Behavior during Evaporation. *Geotechnics* **2022**, 2, 754–764. https://doi.org/10.3390/geotechnics2030036

Academic Editors: Yong Sheng and Kenneth Imo-Imo Israel Eshiet

Received: 28 June 2022
Accepted: 30 August 2022
Published: 2 September 2022

Publisher's Note: MDPI stays neutral with regard to jurisdictional claims in published maps and institutional affiliations.

Copyright: © 2022 by the authors. Licensee MDPI, Basel, Switzerland. This article is an open access article distributed under the terms and conditions of the Creative Commons Attribution (CC BY) license (https://creativecommons.org/licenses/by/4.0/).

1. Introduction

Agricultural farmlands in the semi-arid climate zones of the Canadian prairies are challenged by a scarcity of water [1]. In southern Saskatchewan, an irrigation system based on a surface water reservoir is being planned to operate during regular weather. However, users will have to rely on groundwater in drought years when the water levels are low in the reservoir [2]. Both of these water sources are characterized by elevated concentrations of dissolved solids owing to the salt-rich mineralogy in several stratigraphic units of the regional Phanerozoic basin [3]. Additionally, the use of fertilizers gradually increases the salt concentration in the soil. The interaction of saline water with the soil raises serious concerns with respect to evaporation, especially during the summer farming season. Actual evaporation (AE) involves multiple stages of desaturation through the soil pores within a profile due to decreasing exposure to the atmosphere [4]. Previous studies on AE have generally focused on land–atmosphere interactions [5] and material properties [6] and do not explore the effect of pore fluid on soil behavior [7]. This is especially true in regards to the determination of water retention [8], the associated shrinkage in clays [9], and the correlation of these properties with the process of evaporation. To ensure sustainable agricultural practices, there is a need to explore the influence of pore fluid salinity on evaporative losses in soils.

Evaporative flux from soil is defined as the water mass passing through the surface area per unit time [10]. The determination of actual evaporation from an exposed soil

surface is quite complex. Field studies require a long time commitment and only capture local atmospheric conditions; for example, the lysimeter testing performed over 22 years in Saskatchewan, Canada [11]. Likewise, such studies need extensive instrumentation as indicated by the real-time monitoring of flux boundary conditions in Singapore [12]. Laboratory testing can circumnavigate spatiotemporal variations and can generate data under control conditions [13]. This helps to avoid the pitfalls of site-specific correlations while enabling a comprehensive understanding of the influencing parameters at the soil–atmosphere interface.

From a conceptual viewpoint and starting at initially saturated conditions, soils usually exhibit the following distinct evaporation rates during drying [14]: *Stage I*, highest rate as the surface is covered with a water film to facilitate potential evaporation (PE) [15]; *Stage II*, decreasing rate when air begins to enter the relatively large soil pores to activate capillary flow [16]; *Stage III*, constant rate since the pore network steadily provides water to the surface [17]; *Stage IV*, decreasing rate when the pore system is partially blocked due to entrapped air [18]; and *Stage V*, decreasing rate as vapor transport becomes dominant [19]. These stages exist under low atmospheric demand, that is, PE < 5 mm/day (58 mg/m^2·s) [6]. Under higher atmospheric demand, such as during the summer, *Stage III* becomes absent because of the high exchange of vapor between the atmosphere and the evaporating surface [20].

Evaporation studies on inert soils at high salinity (initially saturated with NaCl solution) indicate that the main phenomenon is salt precipitation: reduced evaporative fluxes due to the development of a salt crust and a high salinity zone above the evaporating front [21]; correlation of the end of *Stage III* evaporation with the highest rate of crust formation [22]; and correlation of temperature and humidity with crustal growth [7]. In contrast, clays interact with the NaCl solution to affect soil behavior during evaporation. For example, reduction in the shrinkage limit at high salinity and increased osmotic suction in kaolinite due to a thinner diffuse double layer and enhanced inter-particle attraction, respectively [23]; increased aggregation of clay platelets due to high colloid–electrolyte interactions in bentonite [24]; excessive time requirement (up to five days) to desaturate a natural expansive soil through oven-drying because salt precipitation narrowed the pore sizes to entrap water [25]; and correlation of osmotic volume change to the rate of migration of dissolved salt through a smectite-rich clay [26]. To date, there is no research that investigates the influence of pore fluid salinity on the desaturation–shrinkage behavior of soils during the entire evaporation process.

The main objective of this research was to investigate the effect of saline pore fluid on soil behavior during evaporation. Evaporative fluxes from inert and active soils were determined under low atmospheric demand to correlate with water retention and soil shrinkage as well as under high atmospheric demand to mimic regional climatic conditions during summer.

2. Research Methodology

Representative soils were retrieved from southern Saskatchewan and included an inert silty sand from Avonlea [27] and an active lean clay from Belle Plaine [28]. The silty sand primarily comprised quartz and feldspar [29], whereas the lean clay had 44% clay minerals such as interstratified corrensite and illite [30]. According to Suchan and Azam [14], the silty sand is poorly graded, with 19% of material finer than 0.075 mm, whereas the lean clay is well-graded with 62% of material finer than 0.075 mm. Material properties (Table 1) were determined using a highly saline solution [31]. The stock solution was prepared by mixing 5500 mg of NaCl with 1 L of distilled water at room temperature (20 °C) for 30 min. For both soil types, the adsorption and retention capabilities slightly decreased at high salinity due to a reduction in double-layer thickness [32].

Table 1. Summary of material properties.

Material Property	ASTM *	Silty Sand		Lean Clay	
		Water **	Saline	Water *	Saline
Pore Fluid					
Dissolved NaCl (ppm)		<10	5500	<10	5500
Fluid Density at 20 °C ($g \cdot cm^{-3}$)		0.998	1.002	0.998	1.002
Soil					
Liquid Limit, w_l (%)	D4318-17e1	27	24	32	29
Plastic Limit, w_p (%)	D4318-17e1	25	23	18	16
Shrinkage Limit, w_s (%)	[24]	-	-	14	13

* American Society for Testing and Materials. ** Data from Suchan and Azam [14].

Low-demand evaporation tests were conducted under ambient laboratory atmosphere using saturated samples. A mortar and pestle were used to break down the soil and the moisture was removed by oven drying at 110 °C for 24 h. The sample cup (18.6 cm^3 internal volume) was evenly filled with 24 g of soil and 9.5 g of saline solution was added to achieve saturated conditions (gravimetric water content $w \approx 40\%$ and volumetric water content $\theta \approx 50\%$) [14]. Following 12 h of homogenization in a sealed container, the sample surface was smoothed to the rim height to eliminate possible swelling. Thereafter, the sample was alternatively placed in an enclosure over a high-precision scale (A&D Apollo GX-603A) to measure mass (at 4 h intervals for up to 16 h and thereafter at 8 h intervals for up to 72 h) and in the controlled photogrammetry system (CPS) for 25 min to determine dimensions of width, height, surface area, and total volume [33]. In contrast, the high demand tests were conducted in the Bench-scale Atmospheric Simulator (BAS2), in which summer day conditions of the Canadian prairies [34] were simulated by controlling the velocity, pressure, temperature and relative humidity of air, solar irradiation, and the temperature of soil [35]. For this purpose, unsaturated samples were prepared by adding 6.7 g of solution to achieve 27% w and 50% θ [14].

Table 2 summarizes the measured atmospheric and surface parameters. The low-demand tests collected more than 9400 data points at 30 s intervals. The air velocity at the soil surface was found to be less than 0.1 m/s because the mass balance had glass side-protectors and a partially covered roof to preclude cross winds. Likewise, the air pressure and relative humidity were measured next to the mass balance and recorded values of about 95 kPa and 28 ± 4%, respectively. The controlled air temperature registered 21 °C. The test samples were mostly kept under dark conditions, except during the 25 min CPS photo sessions, to ensure negligible values for both incoming and outgoing shortwave energy fluxes.

Table 2. Summary of measured atmospheric and surface parameters.

Parameter	Unit	Symbol	Silty Sand		Lean Clay	
			Low Demand	High Demand	Low Demand	High Demand
Data Point Count		n	9410	2161	10,404	2161
Air Velocity	m/s	v	<0.1	1.3	<0.1	1.3
Air Pressure	Pa	e_a	94,752	93,760	94,762	95,055
Relative Humidity	%	h_{UL}	32.0	55.5	23.5	55.2
Air Temperature	°C	T_{aUL}	19.9	19.0	21.5	19.0
Shortwave Flux (↓) *	W/m^2	S_i	0	325	0	325
Shortwave Flux (↑) **	W/m^2	S_o	0	1	0	1
Soil Temperature	°C	T_s	-	22.1	-	22.0

* ↑ upward, ** ↓ downward.

High-demand evaporation tests were conducted under atmospheric conditions prevalent during a typical summer day [34]. Such conditions represented the longest period of evaporation (1755 h out of all 5533 evaporating hours) and the highest rate of potential evaporation (186 $mg/m^2 \cdot s$) in the Canadian prairies [36]. There were about 2160 data points at 10 s intervals. The air velocity was kept at 1.3 m/s. The summer day air pressure was recorded to be 93.9 kPa. Likewise, relative humidity and air temperature measured about 55% and 19.0 °C, respectively. An externally mounted light source in a nadir position above the sample delivered 325 W/m^2 of incoming shortwave energy of the solar spectrum such that 1 W/m^2 was reflected back. The surface temperature was recorded to be 22 °C. These data indicate good precision and repeatability under controlled conditions because spatiotemporal variations in atmospheric parameters and physiographic features were precluded.

The drying water retention curve (WRC) was determined according to the Standard Test Method for Measurement of Soil Potential (Suction) Using Filter Paper (ASTM D5298-16) through the Whatman No. 42 filter paper. This method was selected to ensure simultaneous measurement of total and matric suction over a wide range of soil suction values [37]. The bi-linear calibration curve, given by Greacen et al. [38] and recommended by ASTM, was used to ensure accuracy [39]. Twenty (20) identical samples were saturated with the saline solution and allowed to dry under ambient laboratory conditions (temperature of 19.6 °C $\pm$ 0.4 °C and relative humidity of 21.7% $\pm$ 6.5%). Target gravimetric water contents of 40% to 1% with ten equal increments were selected to capture the entire range of saturated–unsaturated soil behavior. At the desired pore fluid content, the samples were stored inside an insulated box for 30 days to ensure equilibration of the filter paper's water content [40]. Filter papers were then removed and weighed to determine retained water content. Further details on the stepwise procedure for water retention analysis are given in Suchan and Azam [14].

3. Results and Discussion

Figure 1 presents three-dimensional models of silty sand and lean clay over the entire range of drying under ambient atmosphere. The silty sand (Figure 1a) exhibited negligible horizontal and surface area deformation. A fluid film at surface along with a vertical deformation was observed at 4 h after which no further deformation was recorded. Over time, the sample colored changed from dark brown to light brown, indicating the downward movement of the drying front. The lean clay (Figure 1b) exhibited significant vertical deformations up to 24 h, after which lateral deformations became visible. The surface film disappeared by the 4 h observation and the change in color from dark brown to light brown became visible at the 64 h observation.

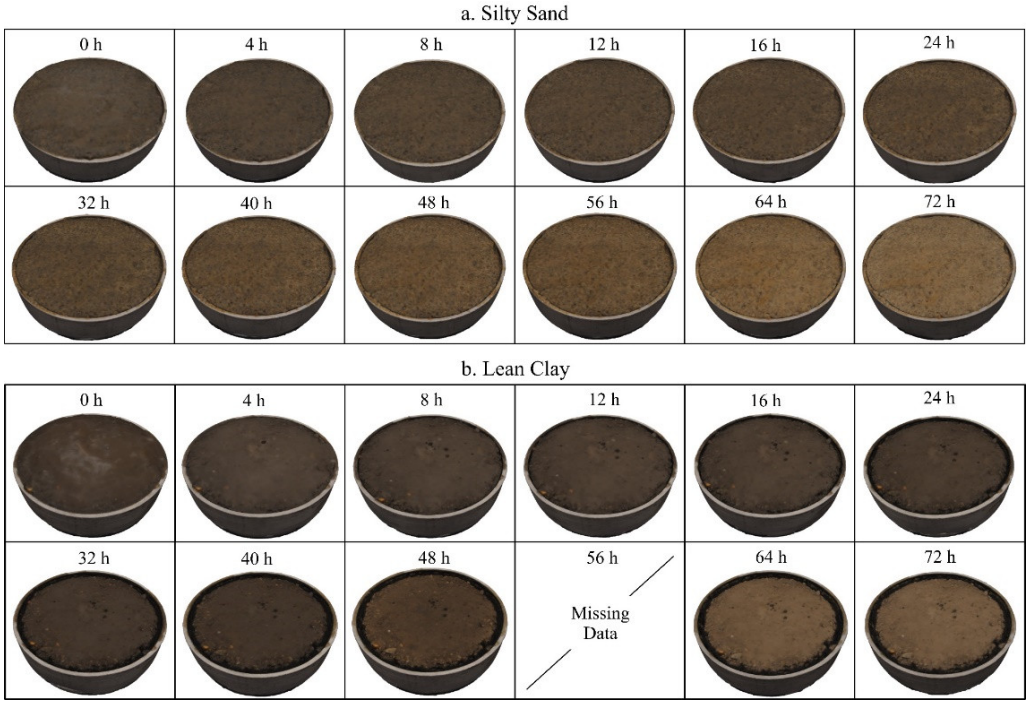

Figure 1. Three-dimensional models of the investigated soils during drying under ambient laboratory conditions: (**a**) silty sand; and (**b**) lean clay.

Figure 2 presents the various types of deformations versus water content for the investigated soils. Four distinct types of soil deformation are presented: (i) horizontal deformation (D_d, %), the ratio of the sample diameter at time t (d_t; mm) to the initial diameter (d_0; mm); (ii) vertical deformation (D_h, %), the ratio of the sample height at time t (h_t) to the initial height (h_0); (iii) surface area deformation (D_s, %), the ratio of the exposed area (including the top and the sides) at time t (s_t) to the initial exposed area at 0 h (s_0); and (iv) volume deformation (D_v, %), the ratio of the total sample volume at time t (v_t) to the initial volume at 0 h (v_0).

The D_d (Figure 2a) of silty sand for both pore fluids was identical because of the inert nature of the soil. In contrast, the D_d of lean clay exhibited three zones, beginning with negligible movement until 35% w, followed by a linear increase to 8% by 8% w, and no change thereafter. This pattern is similar to that under non-saline conditions, although there are higher values of deformation due to a thinner DDL diffuse double layer (DDL) caused by pore fluid ions that increased inter-particular attraction between clay platelets [41]. This means a decrease in electrochemically attached water and an increase in pore water, which is easily removed.

The D_h (Figure 2b) of silty sand increased linearly to 5% by 32% w, followed by negligible change thereafter. In comparison with the non-saline conditions, this sample showed a 1% decrease in vertical movement, which was attributed to salt precipitation within the pore space [42]. In contrast, the lean clay gradually increased to 16% (more than the 13% for the non-saline conditions) due to the above-mentioned mechanism. In this case, salt precipitation is subdued because the pore fluid electrolytes interacted with the clay particle surfaces to reduce DDL thickness.

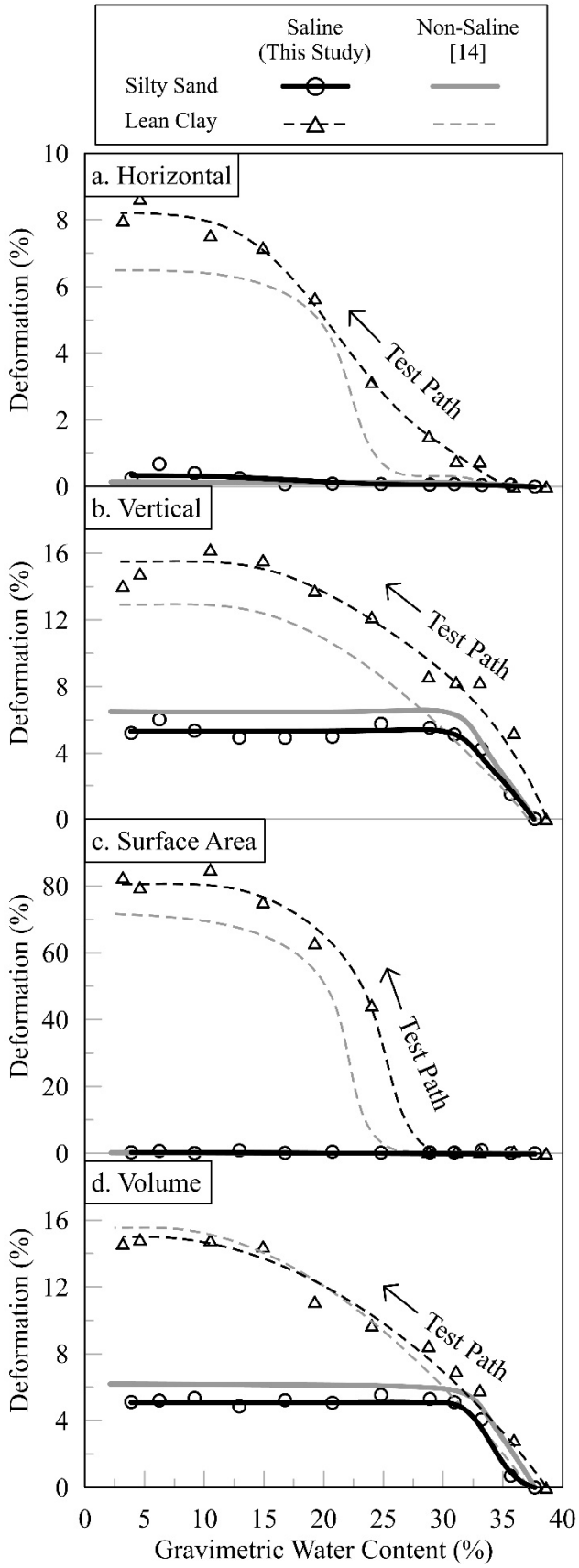

Figure 2. Deformations during drying under low demand for silty sand and lean clay: (**a**) horizontal deformation; (**b**) vertical deformation; (**c**) surface area deformation; and (**d**) volumetric deformation.

The D_s (Figure 2c) of silty sand was similar to the non-saline sample and closely followed D_d, which is attributed to negligible physiochemical interactions. Contrary to this trend, the D_s of lean clay showed negligible movement until 28% w, followed by an increase of up to 80% by 12% w and minimal change thereafter. In addition to physiochemical interactions, the increased D_s is partly attributed to an undulating surface observed during the evaporation process.

Finally, the trend in D_v (Figure 2d) for silty sand was similar to D_h because of the dominance of vertical deformation and a total deformation of 5% was recorded. On the other hand, the trend for the lean clay closely followed that under non-saline conditions and approached a value of 15%. This is attributed to surface undulations and reduced evaporation due to precipitated salts [43].

Figure 3 presents the behavior of silty sand under low atmospheric demand in terms of evaporation, the water retention curve (WRC), soil shrinkage curve (SSC) with respect to gravimetric water content (w), volumetric water content (θ), and degree of saturation (S). *Stage I* and *Stage V* were not captured in evaporation tests. Evaporative flux comprised *Stage II*, which decreased from 26 mg/m^2·s (38% w, 49% θ and 95% S) to 22 mg/m^2·s (28% w, 40% θ, and 83% S), followed by constant flux during *Stage III* at 22 mg/m^2·s until 13% w, 16% θ, and 35% S. The evaporative flux through the soil pores in both of these stages was lower than that for the non-saline conditions. This is attributed to an increased ion concentration gradient (reduced vapor pressure gradient) in the pores [44]. The *Stage IV* evaporative flux was a close match to the non-saline conditions, with a decrease to 13 mg/m^2·s by 6% w, 6% θ, and 18% S. This is largely because an increase in ion concentration results in salt precipitation within the pore spaces (already blocked with entrapped air) thereby inhibiting evaporation [45].

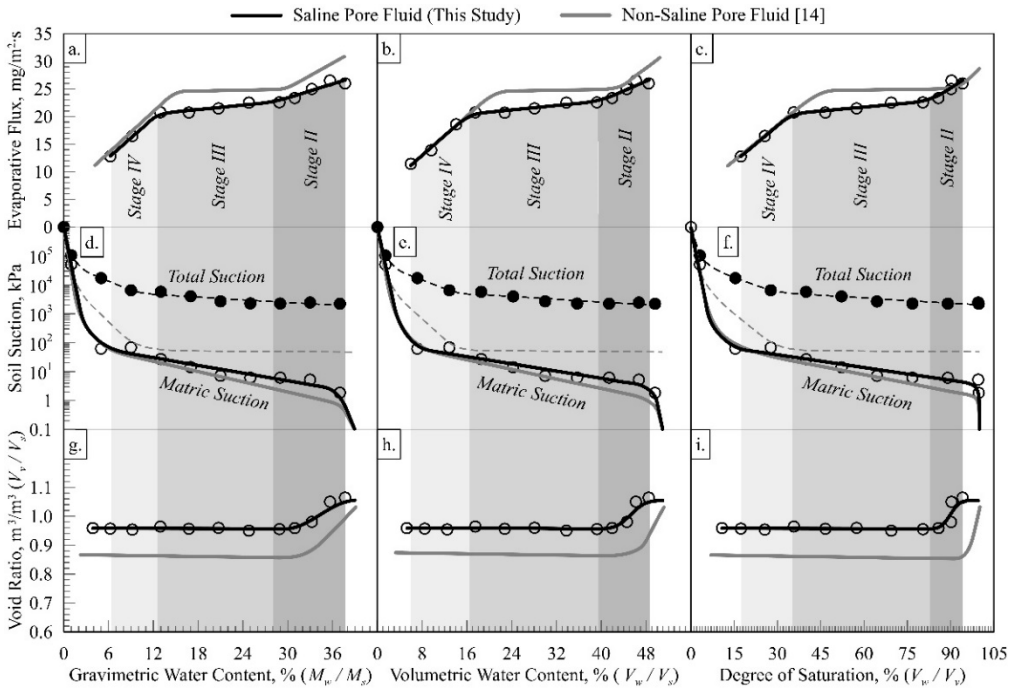

Figure 3. Behavior of silty sand under low atmospheric demand: (**a**) w-based evaporative flux; (**b**) θ-based evaporative flux; (**c**) S-based evaporative flux; (**d**) w-based water retention curve; (**e**) θ-based water retention curve; (**f**) S-based water retention curve; (**g**) w-based soil shrinkage curve; (**h**) θ-based soil shrinkage curve; and (**i**) S-based soil shrinkage curve.

The WRC included matric suction and total suction, whereas osmotic suction was calculated as the difference of the former two values. As expected, the silty sand matric suctions followed a trend similar to the non-saline conditions. The air entry value (AEV)

and the residual suction value (RSV) were found to be 5 kPa and 100 kPa, respectively. The total suction remained near 5000 kPa (up to 10% w, 13% θ, and 26% S) after which it gradually increased to merge with matric suction beyond *Stage IV*. This 70 times increase above the non-saline conditions was due to the osmotic component of total suction derived from the saline pore fluid [46]. Furthermore, the J-shaped SSC trend was similar to the non-saline conditions and comprised a decreasing void ratio from 1.04 to 0.96 within *Stage II* and a flat line thereafter [42]. The higher void ratios in the saline condition are attributed to the precipitation of salt grains, which are finer than the soil particles. This was also observed earlier in the form of decreased D_v (Figure 2d).

Figure 4 presents the behavior of lean clay under low atmospheric demand. Evaporative flux during *Stage II* decreased from 30 mg/m^2·s (39% w, 51% θ, and 100% S) to 15 mg/m^2·s (21% w, 34% θ, and 77% S). This is lower than non-saline conditions because of an increased ion concentration gradient (reduced vapor pressure gradient) in the pores, as mentioned before [44]. The relatively wider range of capillary-supported *Stage III* is attributed to the release of water into the pore spaces owing to a reduced DDL thickness [47]. Furthermore, the evaporative flux gradually decreased during *Stage III* to 10 mg/m^2·s flux (6% w, 9% θ, and 21% S) and then to 5 mg/m^2·s (3% w, 5% θ, and 12% S) in *Stage IV*. In both cases, the trends were similar to the non-saline conditions and are attributed to the previously described phenomena [48].

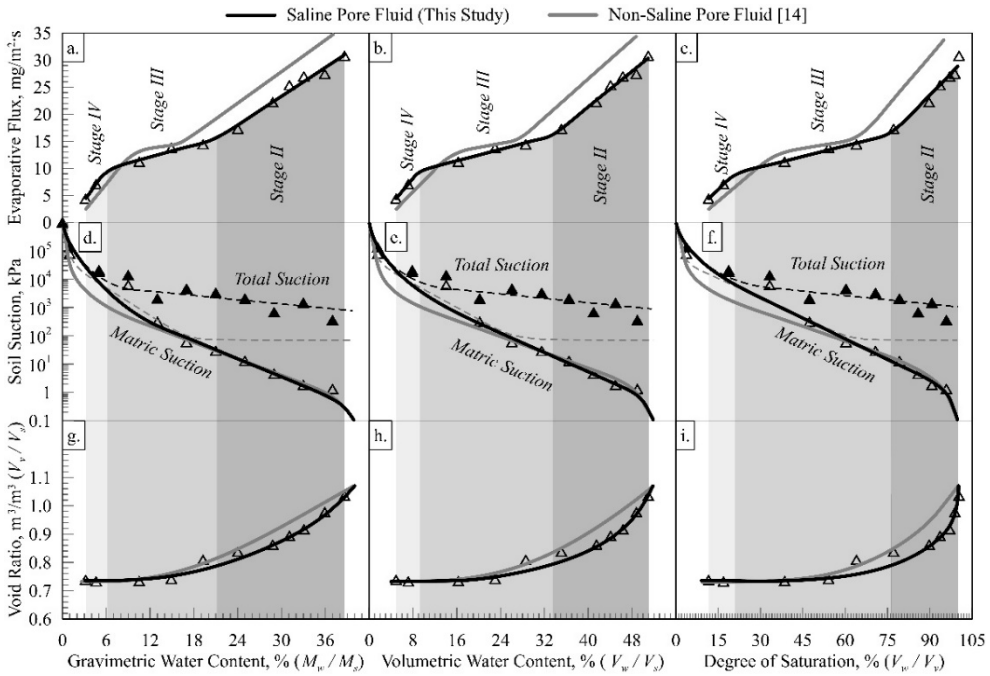

Figure 4. Behavior of lean clay under low atmospheric demand: (**a**) w-based evaporative flux; (**b**) θ-based evaporative flux; (**c**) S-based evaporative flux; (**d**) w-based water retention curve; (**e**) θ-based water retention curve; (**f**) S-based water retention curve; (**g**) w-based soil shrinkage curve; (**h**) θ-based soil shrinkage curve; and (**i**) S-based soil shrinkage curve.

The matric suction trend was similar to in non-saline conditions with negligible changes up to the AEV (5 kPa), followed by a gradual decline up to the RSV (2000 kPa), and then by a straight line up to a completely dry state. The total suction during *Stage II* and *Stage III* ranged from 1000 kPa to 6000 kPa with an average value of 3500 kPa compared to a relatively constant value of 100 kPa for non-saline conditions. This is due to the gradual release of adsorbed water to the void spaces [47]. As before, the total suction merged with the matric suction near the boundary of *Stage III* and *Stage IV*. Finally, the SSC void ratio initially decreased in *Stage II* (1.07 to 0.82), followed by a marginal decrease in *Stage III* (0.82 to 0.73), and finally a flat line (0.73) within *Stage IV*. This follows the trend in non-saline

conditions, as similar D_v (Figure 2d) was attributed to surface undulations and reduced evaporation due to precipitated salts [43].

Figure 5 provides the evaporative fluxes under high demand. In silty sand (Figure 5a), *Stage III* remained a constant flux at 180 mg/m^2·s over a wider range of 28% w to 14% w. This shift is attributed to an increased ion concentration gradient in the capillary pores, as discussed before [44]. In contrast, *Stage IV* followed a similar trend to the non-saline conditions, with a linear decrease to 50 mg/m^2·s by 12% w, similar to the observations by [7]. Again, the reduced evaporation was due to salt precipitation in the already blocked pore spaces thereby inhibiting [45].

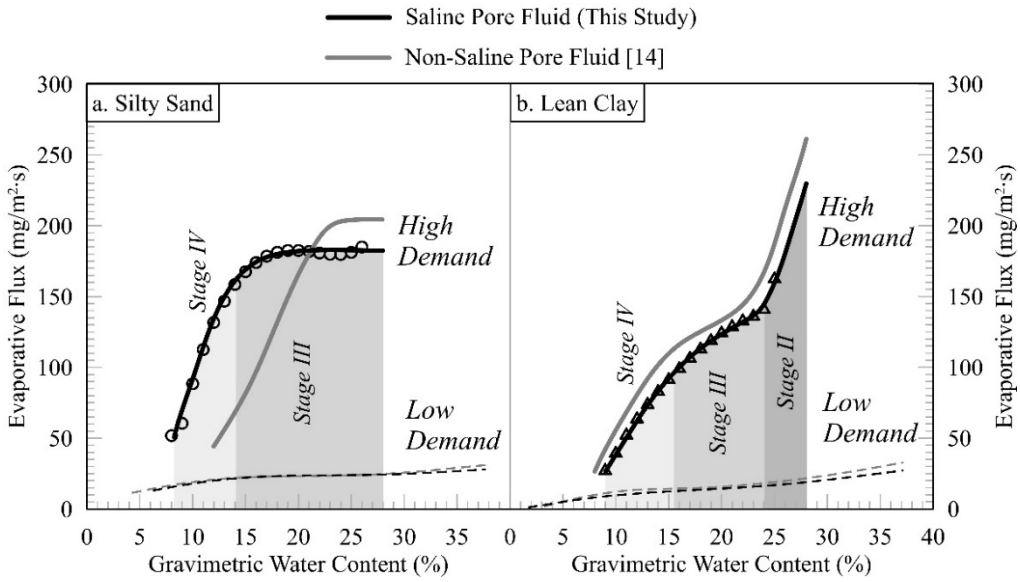

Figure 5. Evaporative flux under high demand for (**a**) silty sand and (**b**) lean clay.

The lean clay (Figure 5b) comprised *Stage II*, in which there was a sharp decrease from 230 mg/m^2·s (28% w) to 145 mg/m^2·s (24% w), *Stage III*, with a moderate decrease to 95 mg/m^2·s by 16% w, and *Stage IV*, with a further decrease up to 25 mg/m^2·s (9% w). This pattern closely matched the non-saline conditions with evaporative flux reduced by about 10 mg/m^2·s. These slightly lower values are attributed to the reasons discussed earlier.

For the investigated range of water content, the total water loss under high demand was six times higher than under low demand. This is lower than the non-saline conditions (seven times higher) and is attributed to the effects of increased pore fluid salinity, as described earlier.

4. Summary and Conclusions

The knowledge of soil behavior under saline conditions is critical to understand evaporative losses from soils. Laboratory tests were conducted on a silty sand and a lean clay with saline pore fluid under low-demand and high-demand atmospheric conditions. The main conclusions of this study are given as follows:

1. Over the investigated range of water content, the sample color change from dark brown to light brown indicated the downward movement of the drying front. The silty sand exhibited negligible horizontal and surface area deformations with 5% vertical and volumetric reductions. The lean clay decreased 8% horizontally and 16% vertically, while the surface area deformed by 80% and the volume reduced by 15%.
2. The silty sand evaporative flux decreased from 26 mg/m^2·s to 22 mg/m^2·s in *Stage II*, remained at a constant flux in *Stage III*, and decreased to 13 mg/m^2·s in *Stage IV*. Based on matric suction, the AEV and RSV were 5 kPa and 100 kPa, respectively. The total suction was about 5000 kPa and merged with matric suction near the *Stage*

II/Stage III boundary. The SSC was J-shaped, with the only void ratio decrease in *Stage II*.

3. The lean clay evaporative flux decreased from 30 mg/m^2·s to 15 mg/m^2·s in *Stage II*, to 10 mg/m^2·s in *Stage III*, and then to 5 mg/m^2·s in Stage *IV*. The AEV was 5 kPa and the RSV was 2000 kPa. The total suction during *Stage II* and *Stage III* ranged from 1000 kPa to 6000 kPa with an average value of 3500 kPa. The SSC showed a major void ratio decrease in *Stage II*, marginal decrease in *Stage III*, and no decrease in *Stage IV*.
4. Under high demand, the evaporative flux for silty sand was constant at 180 mg/m^2·s in *Stage III* and decreased to 50 mg/m^2·s in *Stage IV*. The lean clay decreased from 230 mg/m^2·s to 145 mg/m^2·s in *Stage II*, to 95 mg/m^2·s in *Stage III*, and to 25 mg/m^2·s in *Stage IV*. For both soils, the total water loss was found to be six times that under low demand.

Author Contributions: Data curation and analysis, J.S.; Supervision, S.A.; Writing—original draft, J.S.; Writing—review and editing, S.A. All authors have read and agreed to the published version of the manuscript.

Funding: This research was funded by Natural Science and Engineering Research Council of Canada.

Acknowledgments: The authors would like to thank the University of Regina for providing laboratory space.

Conflicts of Interest: The authors declare there is no conflict of interest.

References

1. Sauchyn, D.; Kennedy, S.; Stroich, J. Drought, climate change, and the risk of desertification on the Canadian prairies. *Prairie Forum* **2005**, *30*, 143–156.
2. Joly, M. *Prairie Prosperity*, 1st ed.; Government of Canada: Ottawa, ON, Canada, 2020.
3. Florinsky, I.V.; Eilers, R.G.; Wiebe, B.H.; Fitzgerald, M.M. Dynamics of soil salinity in the Canadian prairies: Application of singular spectrum analysis. *Environ. Model. Softw.* **2009**, *24*, 1182–1195. [CrossRef]
4. Shuttleworth, W.J. Evaporation. In *Handbook of Hydrology*, 1st ed.; Maidment, D.R., Ed.; McGraw-Hill Inc.: New York, NY, USA, 1993; Volume 1, pp. 4.1–4.53.
5. Kobayashi, T.; He, W.; Nagai, H. Mechanisms of evaporation from soil with a dry surface. *Hydrol. Processes* **1998**, *12*, 2185–2191. [CrossRef]
6. Or, D.; Lehmann, P.; Shahraeeni, E.; Shokri, N. Advances in Soil Evaporation Physics-A Review. *Vadose Zone J.* **2013**, *12*, 1–16. [CrossRef]
7. Shokri-Kuehni, S.M.S.; Rad, M.N.; Webb, C.; Shokri, N. Impact of type of salt and ambient conditions on saline water evaporation from porous media. *Adv. Water Resour.* **2017**, *105*, 154–161. [CrossRef]
8. Spears, M.; Huntington, J.; Subhrendu, G. *Improving Reservoir Evaporation Estimates*; U.S. Department of the Interior, Bureau of Reclamation Research and Development Office: Denver, CO, USA, 2016; Volume 1, pp. 1–63.
9. Khan, F.S.; Azam, S. Spatial variability in swelling of aggregated expansive clays. *Innov. Infrastruct. Solut.* **2016**, *1*, 1–6. [CrossRef]
10. Wilson, G.W.; Fredlund, D.; Barbour, S. Coupled soil-atmosphere modelling for soil evaporation. *Can. Geotech. J.* **1994**, *31*, 151–161. [CrossRef]
11. Staple, W. Evaporation from soil and vegetation. *Neth. J. Agric. Sci.* **1956**, *4*, 39–42. [CrossRef]
12. Rahardjo, H.; Nio, A.S.; Harnas, F.R.; Leong, E. Comprehensive Instrumentation for Real Time Monitoring of Flux Boundary Conditions in Slope. *Procedia Earth Planet. Sci.* **2014**, *9*, 23–43. [CrossRef]
13. Trautz, A.C.; Illangasekare, T.H.; Howington, S. Experimental Testing Scale Considerations for the Investigation of Bare-Soil Evaporation Dynamics in the Presence of Sustained Above-Ground Airflow. *Water Resour. Res.* **2018**, *54*, 8963–8982. [CrossRef]
14. Suchan, J.; Azam, S. Influence of Desaturation and Shrinkage on Evaporative Flux from Soils. *Geotechnics* **2022**, *2*, 412–426. [CrossRef]
15. Wilson, G.W.; Fredlund, D.G.; Barbour, S.L. The effect of soil suction on evaporative fluxes from soil surfaces. *Can. Geotech. J.* **1997**, *34*, 145–155. [CrossRef]
16. Le Bray, Y.; Prat, M. Three-dimensional pore network simulation of drying in capillary porous media. *Int. J. Heat Mass Transf.* **1999**, *42*, 4207–4224. [CrossRef]
17. An, N.; Tang, C.-S.; Xu, S.-K.; Gong, X.-P.; Shi, B.; Inyang, H.I. Effects of soil characteristics on moisture evaporation. *Eng. Geol.* **2018**, *239*, 126–135. [CrossRef]
18. Lehmann, P.; Assouline, S.; Or, D. Characteristic lengths affecting evaporative drying of porous media. *Phys. Rev. E* **2008**, *77*, 056309. [CrossRef]

19. Yiotis, A.G.; Tsimpanogiannis, I.N.; Stubos, A.K.; Yortsos, Y.C. Pore-network study of the characteristic periods in the drying of porous materials. *J. Colloid Interface Sci.* **2006**, *297*, 738–748. [CrossRef]
20. Shahraeeni, E.; Lehmann, P.; Or, D. Coupling of evaporative fluxes from drying porous surfaces with air boundary lay-er: Characteristics of evaporation from discrete pores. *Water Resour. Res.* **2012**, *48*, W09525. [CrossRef]
21. Gran, M.; Carrera, J.; Massana, J.; Saaltink, M.W.; Olivella, S.; Ayora, C.; Lloret, A. Dynamics of water vapor flux and water sepa-ration processes during evaporation from a salty dry soil. *J. Hydrol.* **2011**, *396*, 215–220. [CrossRef]
22. Rad, M.N.; Shokri, N. Nonlinear effects of salt concentrations on evaporation from porous media. *Geophys. Res. Lett.* **2012**, *39*. [CrossRef]
23. Mishra, P.N.; Scheuermann, A.; Bore, T.; Li, L. Salinity effects on soil shrinkage characteristic curves of fine-grained geomaterials. *J. Rock Mech. Geotech. Eng.* **2018**, *11*, 181–191. [CrossRef]
24. Zhang, T.; Deng, Y.; Cui, Y.; Lan, H.; Zhang, F.; Zhang, H. Porewater salinity effect on flocculation and desiccation cracking behaviour of kaolin and bentonite considering working condition. *Eng. Geol.* **2019**, *251*, 11–23. [CrossRef]
25. Ho, Y.A.; Pufahl, D.E. The effects of brine contamination on the properties of fine-grained soils. In *Geotechnical Special Publication No. 13. Geotechnical Practice for Waste Disposal '87*; American Society of Civil Engineers: New York, NY, USA, 1987; pp. 547–561.
26. Barbour, S.L.; Fredlund, D.G. Mechanisms of osmotic flow and volume change in clay soils. *Can. Geotech. J.* **1989**, *26*, 551–562. [CrossRef]
27. Azam, S.; Khan, F. Geohydrological properties of selected badland sediments in Saskatchewan, Canada. *Bull. Eng. Geol. Environ.* **2013**, *73*, 389–399. [CrossRef]
28. Paranthaman, R.; Azam, S. Effect of compaction on desiccation and consolidation behavior of clay tills. *Innov. Infrastruct. Solutions* **2021**, *7*, 1–8. [CrossRef]
29. Khan, F. *Engineering Properties of Badlands in Semi-Arid Regions*; University of Regina: Regina, SK, Canada, 2012.
30. Paranthaman, R.; Azam, S. Effect of Composition on Engineering Behavior of Clay Tills. *Geosciences* **2021**, *11*, 427. [CrossRef]
31. Smith, J.L.; Doran, J.W. Measurement and use of pH and electrical conductivity for soil quality analysis. *Methods Assess. Soil Qual.* **1997**, *49*, 169–182.
32. Mishra, P.N.; Scheuermann, A.; Li, L. Significance of Corrections and Impact of Saline Pore Fluid on Kaolin. *J. Mater. Civ. Eng.* **2018**, *30*, 06018016. [CrossRef]
33. Suchan, J.; Azam, S. Controlled photogrammetry system for determination of volume and surface features in soils. *MethodsX* **2021**, *8*, 101368. [CrossRef]
34. Suchan, J.; Azam, S. Determination of Evaporative Fluxes Using a Bench-Scale Atmosphere Simulator. *Water* **2021**, *13*, 84. [CrossRef]
35. Suchan, J.; Azam, S. Development of BAS2 for determination of evaporative fluxes. *MethodsX* **2021**, *8*, 101424. [CrossRef]
36. Suchan, J.; Azam, S. Effect of Salinity on Evaporation from Water Surface in Bench-Scale Testing. *Water* **2021**, *13*, 2067. [CrossRef]
37. Suits, L.D.; Sheahan, T.; Leong, E.; He, L.; Rahardjo, H. Factors Affecting the Filter Paper Method for Total and Matric Suction Measurements. *Geotech. Test. J.* **2002**, *25*, 8198. [CrossRef]
38. Greacen, E.L.; Walker, G.R.; Cook, P.G. *Procedure for Filter Paper Method of Measuring Soil Water Suction*; CSIRO Division of Soils: Adelaide, Australia, 1987.
39. Kim, H.; Prezzi, M.; Salgado, R. Calibration of whatman grade 42 filter paper for soil suction measurement. *Can. J. Soil Sci.* **2016**, *97*, 93–98. [CrossRef]
40. Bulut, R.; Leong, E.C. Indirect measurement of suction. *Geotech. Geol. Eng.* **2008**, *26*, 633–644. [CrossRef]
41. Narashimha Rao, S.; Mathew, P.K. Effects of exchangeable cations on hydraulic conductivity of a marine clay. *Clays Clay Miner.* **1995**, *43*, 433–437.
42. Jambhekar, V.; Helmig, R.; Schroder, N.; Shokri, N. Free-Flow–Porous-Media Coupling for Evaporation-Driven Transport and Precipitation of Salt in Soil. *Transp. Porous Media* **2015**, *110*, 251–280. [CrossRef]
43. Peng, X.; Horn, R.; Deery, D.; Kirkham, M.B.; Blackwell, J. Influence of soil structure on the shrinkage behaviour of a soil irrigated with saline—sodic water. *Soil Res.* **2005**, *43*, 555–563. [CrossRef]
44. Mishra, P.N.; Liu, A.; Bore, T.; Scheuermann, A.; Li, L. Impact of pore fluid salinity on progressive volume change be-havior of kaolin. In Proceedings of the 7th International Conference on Unsaturated Soils (UNSAT-2018), Hong Kong, 3–5 August 2018.
45. Nachshon, U.; Weisbrod, N.; Dragila, M.I.; Grader, A. Combined evaporation and salt precipitation in homogeneous and heterogeneous porous media. *Water Resour. Res.* **2011**, *47*, W03513. [CrossRef]
46. Dunmola, A.S. Predicting Evaporative Fluxes in Saline Soil and Surface-Deposited Thickened Mine Tailings. Ph.D. Thesis, Carleton University, Ottawa, ON, Canada, 2018.
47. Yao, C.; Wei, C.; Ma, T.; Chen, P.; Tian, H. Experimental Investigation on the Influence of Thermochemical Effect on the Pore–Water Status in Expansive Soil. *Int. J. Géoméch.* **2021**, *21*, 04021080. [CrossRef]
48. Shokri-Kuehni, S.M.S.; Vetter, T.; Webb, C.; Shokri, N. New insights into saline water evaporation from porous media: Complex interaction between evaporation rates, precipitation, and surface temperature. *Geophys. Res. Lett.* **2017**, *44*, 5504–5510. [CrossRef]